QUARTERLY JOURNAL OF THE ROYAL METEOROLOGICAL SOCIETY
Q. J. R. Meteorol. Soc. **134**: 1143–1154 (2008)
Published online in Wiley InterScience
(www.interscience.wiley.com) DOI: 10.1002/qj.278

The impact of aerosols on non-precipitating marine stratocumulus. I: Model description and prediction of the indirect effect

A. A. Hill,[a]* S. Dobbie[a] and Y. Yin[b]
[a] *School of Earth and Environment, University of Leeds, UK.*
[b] *Nanjing University of Information Science and Technology, China.*

ABSTRACT: In this paper, the first of a two-part study, we use the UK Met Office large-eddy simulation model (LEM) with fully integrated size-bin-resolved cloud microphysics (BR-LEM) to investigate the effects of increasing cloud condensation nuclei (CCN) concentrations on non-precipitating marine stratocumulus. It is shown, as expected, that increasing CCN concentrations produces an increase in cloud-drop number concentration and a decrease in cloud-drop effective radius. However, for the case presented, we demonstrate that increasing CCN concentrations causes an increase in the rate of evaporative cooling at the cloud top, which drives stronger boundary-layer dynamics, leading to more cloud-top entrainment, which results in a reduction in boundary-layer relative humidity and a reduction in LWP with increasing CCN. Comparison of the BR-LEM simulations with LEM simulations that employ a simpler single-moment bulk scheme (Bulk-LEM) show that the bulk microphysics scheme fails to simulate this CCN–entrainment feedback and the associated reduction in liquid water path. It is shown that, for a very polluted case, the failure of the bulk microphysics to capture this evaporation–entrainment feedback results in a 60% overestimation of the indirect forcing estimate compared to the BR-LEM. We conclude that it is necessary to realistically simulate the dynamic feedbacks associated with increased CCN, otherwise the indirect will be overestimated. Copyright © 2008 Royal Meteorological Society

KEY WORDS large-eddy simulation; bin-microphysics; radiative forcing

Received 13 August 2007; Revised 15 May 2008; Accepted 23 May 2008

1. Introduction

In recent decades, it has become apparent that, in addition to increases in greenhouse gas concentrations, human activities have led to an increase in the mean global burden of radiatively important aerosols. Aerosols influence the Earth's radiation budget (ERB), and hence climate, through several mechanisms. First, aerosols directly alter scattering and absorption of incoming solar radiation, a process which is known as the direct aerosol effect. Although it is generally believed that this exerts a cooling effect on the Earth's surface, absorbing aerosol can cause a warming of the atmosphere, which in turn can influence atmospheric dynamics (e.g. Ramanathan *et al.*, 2001).

Second, aerosols influence ERB indirectly through the fundamental role they play in cloud microphysics and cloud optical properties. Hygroscopic aerosols, such as sulphate, can act as cloud condensation nuclei (CCN) and, if all else is equal, increases in the concentration of CCN causes an increase in the cloud-drop number concentration, N_d, which in turn results in a reduction in cloud-drop size, an increase in cloud optical depth, τ, and an increase in cloud reflectance. This is known as the first indirect aerosol effect (Twomey, 1991). The reduction in cloud-drop size associated with increasing aerosol concentrations causes a reduction in the cloud-drop collision–coalescence and hence a suppression in precipitation, which may result in an enhancement of cloud lifetime, a process known as the second indirect effect (Albrecht, 1989). It is believed that for climatically important low-level clouds, such as marine stratocumulus (Sc), the indirect aerosol effect will cool the planetary system, however the magnitude of this cooling effect is very uncertain (IPCC, 2007).

Finally, an increase in the absorption of solar radiation, which results from the direct effect of increased atmospheric loading of absorbing aerosols, can modify the thermodynamic structure of the atmosphere, which in turn can lead to changes in cloud amount and cloud liquid water content. This is known as the semi-direct effect (e.g. Hansen *et al.*, 1997; Ackerman *et al.*, 2000; Johnson *et al.*, 2004). While the magnitude of the indirect forcing is uncertain, both the magnitude and the sign of the semi-direct forcing are uncertain.

In an attempt to understand the underlying processes of both the indirect and semi-direct effects, and hence reduce the uncertainty in forcing estimates,

* Correspondence to: A. A. Hill, Met Office, FitzRoy Road, Exeter, EX1 3PB, UK. E-mail: adrian.hill@metoffice.gov.uk

some recent studies have employed high-resolution large-eddy simulation (LES) models coupled with cloud microphysical schemes of varying complexity to examine aerosol effects on low-level clouds. For example, both Wang *et al.* (2003) and Ackerman *et al.* (2004) used LES with detailed size-bin-resolved cloud microphysical schemes to investigate the role of aerosols in non-precipitating nocturnal marine Sc (Wang *et al.*, 2003) and precipitating marine Sc (Ackerman *et al.*, 2004). Both these studies demonstrated that increasing aerosol concentrations can lead to dynamical feedbacks that impact the cloud liquid water path (LWP), and thus impact the estimate of the indirect forcing.

Ackerman *et al.* (2000), Johnson *et al.* (2004) and McFarquhar and Wang (2006) used LES with simpler bulk water cloud microphysical schemes to investigate the semi-direct effect. These studies showed that the magnitude of the semi-direct forcing is dependent on the concentration of absorbing aerosol (e.g. Johnson *et al.*, 2004) and cloud type (e.g. Ackerman *et al.*, 2000; Johnson *et al.*, 2004), while the sign of the semi-direct forcing is dependent on the vertical distribution of absorbing aerosol (e.g. Johnson *et al.*, 2004; McFarquhar and Wang, 2006). Although these investigations have given us valuable insight into the processes by which absorbing aerosol influence low-level clouds, they have all employed single-moment bulk water schemes to represent cloud microphysics. In such bulk water schemes, microphysical properties, e.g. N_d and cloud-drop effective radius, r_e, were either fixed in space and time or parametrized from observations. This means that previous research was unable to assess the full cloud microphysical response associated with absorbing aerosol. Furthermore, the bulk microphysics schemes employed did not include aerosol–cloud interactions. Thus, assessment of the indirect effect and hence the net aerosol effect were limited.

In this series of papers, we address these issues by fully integrating a size-bin-resolved cloud microphysical scheme into the UK Met Office (UKMO) large-eddy simulation model (LEM). To distinguish this new model from the standard LEM, the new model is called the bin-resolved LEM (BR-LEM). The BR-LEM is employed to investigate the indirect and semi-direct effects in diurnally varying non-precipitating marine Sc. In this paper, we present a description of the BR-LEM and its development (Section 2). We then present a series of simulations performed with the BR-LEM, which are designed to investigate the indirect effect (Section 3). Although, the main focus of Section 3 is the assessment of the BR-LEM results, we also present results from the standard UKMO LEM with single-moment bulk microphysics (Bulk-LEM) to understand whether the detail of bin microphysics is required. Finally, we present results from radiative forcing experiments for the BR-LEM and Bulk-LEM results (Section 5).

2. Model description

2.1. UKMO LEM

The UKMO LEM is a high-resolution, anelastic, non-hydrostatic numerical model, with equations for momentum conservation, mass continuity and thermodynamics. The LEM explicitly resolves large-scale turbulent motions, which are responsible for most of the turbulent energy and transport of flow, while parametrizing sub-grid processes with a first-order turbulence scheme. The details of the LEM are presented in Gray *et al.* (2001) and will not be described further here, other than a brief description of the microphysical scheme.

The standard UKMO LEM represents warm-phase clouds with a single-moment bulk water scheme in which processes are modelled using mass. This scheme is an 'all-or-nothing' condensation–evaporation scheme in which all excess moisture in supersaturated air is instantaneously converted to liquid water, and likewise any liquid water in sub-saturated air will be converted to vapour. In this scheme, N_d is assumed to be fixed and the cloud-drop size distribution is represented by a gamma function. From here the standard LEM will be referred to as the Bulk-LEM.

2.2. Bin-resolved LEM (BR-LEM)

As part of this work, we have enhanced the microphysical detail simulated by the LEM by fully integrating the detailed size-bin-resolved cloud microphysical scheme developed by Tzivion *et al.* (1987) and Feingold *et al.* (1988). The bin-resolved microphysics scheme simulates the evolution of a cloud-drop spectrum from aerosol through to rain. Aerosol number, cloud-drop mass and cloud-drop number are divided into a size-resolved spectrum. In this work, we use 14 bins to represent aerosol distribution, while the cloud-drop spectrum is divided into 25 size bins for N_d and 25 bins for cloud-drop mass, with mass doubling for adjacent bins i.e. $ms_{k+1} = 2ms_k$, where is k is bin number (1, 2, ..., 25), and ms is the single drop mass for the lower boundary of k. The masses for the lower boundary of the first bin (ms_1) and the upper boundary of the 25th bin ($2 \times ms_{25}$) are 0.1598×10^{-13} and 0.2681×10^{-6} kg, respectively, which correspond to drop diameters of 3.125 and 800 μm. The microphysical processes included in this detailed cloud microphysics scheme are aerosol activation to cloud drops, diffusional growth and decay by condensation and evaporation, cloud-drop collision–coalescence, breakup and sedimentation (Tzivion *et al.*, 1987, 1989; Feingold *et al.*, 1988).

As the focus of this study is the impact of aerosols on non-precipitating processes, i.e. aerosol activation/regeneration and condensation/evaporation, the model presented in this study is an idealised version of the BR-LEM, which neglects precipitation processes (collision–coalescence, breakup and sedimentation). Details of condensation/evaporation are presented in Tzivion

DOI: 10.1002/qj

et al. (1989) while details of the aerosol activation and regeneration scheme are presented below.

2.4. Aerosol activation

In the BR-LEM configuration employed in this work, aerosols are represented by a size-bin-resolved distribution, where the number of bins and the shape of the distribution are chosen by the user. All aerosols are tracked by their dry size and all can act as CCN, thus all microphysically active aerosol are referred to as CCN. In a similar method to that described in Yin *et al.* (2000), activation of CCN to cloud drops is parametrized by using Köhler theory to evaluate whether dry CCN can activate in the ambient conditions. The first stage of this method is to calculate the critical supersaturation, S_{crit}, for a given dry aerosol radius (Yin *et al.* (2000) gives details). CCN activation occurs when the ambient supersaturation is greater than S_{crit} for that CCN radius. This method assumes that the resulting cloud-drop size is the equilibrium size at 100% relative humidity for the CCN. This assumption can be problematic as the equilibrium size of large aerosol can be several tens of microns larger than the aerosol's dry size, i.e. large enough to initiate preciptation processes, yet it can take hours or even days for a large aerosol to attain its equilibrium size (Khain *et al.*, 2000). In contrast, small particles attain a smaller equilibrium size more rapidly than the large aerosol as they need to take up much less liquid water than large particles. Therefore, the parametrization of CCN activation needs to include a time-scale of growth that is representative of the model time step, and hence limit the growth of the large aerosol due to activation.

In the BR-LEM this is done by using a similar method to that described in Yin *et al.* (2000). In this scheme, if a CCN has a dry radius smaller than 0.12 μm it is assumed that within a time step it will grow to its equilibrium size, as calculated by the Köhler theory. On activation these small CCN are transferred to the smallest bin for cloud drops. For CCN larger than 0.12 μm, a correction factor, k, is used to limit the growth of larger aerosol to a smaller non-equilibrium size that is more representative of the size achieved in the model time step. The k factor is calculated using the method described in Yin *et al.* (2000), which is based on the method originally described in Ivanova *et al.* (1977).

This activation scheme is similar to that described by Yin *et al.* (2000), however whereas Yin *et al.* (2000) used predetermined k factors, we have explicitly incorporated the Ivanova *et al.* (1977) method into the BR-LEM so that k factors are calculated using the simulated vertical velocities. The reason for doing this is that while clouds with large updraughts, e.g. cumulus, are fairly insensitive to the choice of the k, i.e. choosing a k factor of 3, 5 or 8 gives very similar results (Ivanova *et al.*, 1977), clouds with low updraughts, e.g. marine Sc, are sensitive (Kogan, 1991). Therefore, by fully incorporating the method of Ivanova *et al.* (1977) into the BR-LEM, we have developed a flexible, non-cloud-specific warm-phase aerosol activation scheme.

2.4. Aerosol recycling

If a cloud drop is not transported to the surface, then its fate will be complete evaporation in sub-saturated air, which will lead to the regeneration of a CCN. Regenerated CCN can form a significant part of the ambient aerosol concentration (Yin *et al.*, 2005) and ignoring this regenerated CCN can result in an unrealistic decline in CCN numbers, which can impact cloud evolution. To prevent this, we have incorporated a CCN regeneration scheme into the BR-LEM, which is based on Kogan *et al.* (1995). This scheme assumes that large CCN particles grow to large cloud drops, which evaporate less efficiently than small cloud droplets. As a result, smaller CCN are liberated first through the evaporation of smaller droplets. Hence, the regenerated CCN fill in the previously activated bins by starting with the smaller bins. Once the CCN number for the smallest bin is restored to its original number concentration, the next largest bin is replenished. This process continues until either all regenerated CCN are replenished back to the CCN distribution or the CCN distribution is returned back to its original state.

It was found that this scheme on its own may not conserve CCN, as the transport of cloud drops can lead to evaporation in regions where there has been no CCN activation, i.e. regions where the CCN distribution may be 'full'. To prevent the loss of these 'excess' CCN, we have incorporated a scheme that allows them to replenish as a log-normal distribution based on the original CCN distribution. A constraint of this scheme is that CCN can only be replenished to a bin if the *domain-averaged* CCN number for that bin is less than the initial CCN number for that bin, which means that the domain-averaged CCN distribution is conserved.

2.5. Radiation model

To calculate radiative fluxes and heating rates, the Fu and Liou (1993) δ-four-stream radiative transfer code has been integrated into both Bulk-LEM and BR-LEM. Dobbie and Jonas (2001) provide details of the Fu and Liou (1993) radiative transfer code in the LEM. The microphysical variables required by the Fu and Liou (1993) code are cloud LWC and cloud-drop r_{e}. When using the Bulk-LEM, r_{e} is specified by the user at the beginning of the simulation. In the BR-LEM, r_{e} is calculated using mass and number from the bin microphysical scheme as described in Yin *et al.* (2000). When the r_{e} is prognosed from the detailed bin scheme, the radiative transfer calculations are dependent on the cloud-drop distribution, which results from microphysics, dynamics and initial CCN distribution. This dependence allows for spatial and temporal variation of r_{e} during the cloud evolution, something that does not occur in the Bulk-LEM.

DOI: 10.1002/qj

3. Simulation of the indirect effect

3.1. Model set-up and initiation

To examine the indirect effect we simulate a case of diurnally varying marine Sc, which is based on observations from the First International Satellite Cloud Climatology Project (FIRE; Hignett, 1991) that was conducted in the summer of 1987. The initial conditions (Table I) are similar to those presented in Johnson *et al.* (2004), which were derived from six radiosonde ascents through the stratocumulus layer during the observation of a diurnal cycle in stratocumulus on 14–15 July. Total water mixing ratio, q_t, and liquid water potential temperature, θ_l, are constant up to 600 m, which is indicative of a well-mixed boundary layer. At the top of this well-mixed layer there is a sharp inversion of 12 K. The inversion corresponds with both the top of the well-mixed layer and the cloud top. Following Johnson *et al.* (2004), a cooling rate of 1 K day^{-1} was applied to take account of the large-scale heat divergence.

In addition to q_t and θ_l, the BR-LEM is initialised with a single-mode log-normal CCN distribution, in which the mean CCN radii is 0.1 μm and the standard deviation is 1.5 (based on Ackerman *et al.*, 2004 and Feingold *et al.*, 2005). The CCN are assumed to consist of only ammonium sulphate, which has a solubility fraction of 1 (i.e. no insoluble material), a density of 1.8 gm^{-3}, and dissociation leads to the liberation of three ions. We performed five simulations of the case that is introduced above, in which initial CCN concentration is explicitly increased from 100 cm^{-3} (clean, control) to 1000 cm^{-3} (very polluted) (Table II). The range of CCN concentrations employed in these simulations spans the range of observations for clean to polluted marine boundary layers (e.g. Raes *et al.*, 2000) and is similar to the range used in other marine Sc modelling studies (e.g. Lu and Seinfeld, 2005). The initial vertical distribution of CCN for all these simulations is constant with height. Upon activation, CCN are scavenged and thus during the simulation the vertical distribution of CCN is inhomogeneous with height.

All simulations are performed in 2D to reduce computational expense. The horizontal domain is 2.5 km with grid resolution of 50 m, while the vertical domain is 12 km and the vertical resolution varies with height, with a resolution of 5 m around the height of the inversion. Such a fine resolution is required to better resolve the cloud-top mixing processes and mixing across the inversion. Above the cloud top the vertical grid is gradually stretched, and hence the vertical resolution is reduced. A large vertical domain is employed so that gaseous absorption and emission of long-wave and short-wave radiation can be properly represented in the Fu and Liou (1993) radiative transfer scheme.

Table I. Initial conditions for all simulations.

Height (m)	q_t(g kg^{-1})	θ_l (K)
0	9.6	287.5
595	9.6	287.5
605	6.6	299.5
900	6.6	301.8
1600	6.0	304.2
12000	0.037	352.2

Table II. Summary of the microphysical settings used to simulate the indirect aerosol effect.

Model	Simulation	CCN conc. (cm^{-3})	r_e (μm)
BR-LEM	Bin100	100	–
	Bin250	250	–
	Bin500	500	–
	Bin750	750	–
	Bin1000	1000	–
Bulk-LEM	Bulk10	–	10
	Bulk7.4	–	7.4
	Bulk6.4	–	6.4
	Bulk5.65	–	5.65
	Bulk5.5	–	5.5

The subsidence rate is given by $W_{subs} = -Dz$, where z is height and D is the large-scale divergence rate. D is 5.5×10^{-6} s^{-1}, which produces a subsidence rate that roughly maintains a steady boundary-layer depth. The lateral boundary conditions are periodic, while the domain top and bottom are rigid lids, such that $w = 0$. The surface fluxes are derived from Monin–Obukhov similarity theory, assuming a no-slip surface and a specified sea surface temperature of 288 K.

Radiative fluxes and heating rates are calculated every three minutes, using the LWC and r_e produced by the bin microphysics scheme. The simulation time for all simulations is 44 hours, which means that both simulations encompass two days and one full night. The Fu and Liou (1993) radiation module was set up to simulate both long-wave and short-wave radiative transfer, by using a time-varying solar zenith angle calculated for 14–15 July 1987 for location 33°N, 119°W, which is consistent with the location and date of the FIRE observations (Hignett, 1991).

Finally, for comparison purposes, we present results from simulations performed with the standard Bulk-LEM (Section 2.1). Unlike the BR-LEM, the Bulk-LEM has no representation of CCN and hence the impact of enhanced CCN concentrations on cloud microphysics has to be approximated. This is done by reducing the cloud-drop r_e from a clean value of 10 μm to the most polluted value of 5.5 μm (Table II). The r_e values used in the Bulk-LEM simulations represent the daytime, i.e. sunlit hours, mean cloud-top r_e diagnosed from the BR-LEM experiments, e.g. the r_e of 7.4 μm used in Bulk7.4, represents the mean cloud-top r_e from Bin250, while Bulk6.4 uses the mean cloud-top r_e from Bin500. These r_e values, along with the LWC calculated in the Bulk-LEM, were used in the radiative calculations for the Bulk-LEM simulations. Comparison of the Bulk-LEM and BR-LEM experiments

DOI: 10.1002/qj

has been used to understand the impact of allowing for the extra detail of the BR-LEM for simulating the first indirect effect in marine Sc, as well as assessing whether assuming a fixed r_e is valid.

3.2. Results and discussion

Figure 1 shows that all simulations produce a diurnal cycle in which LWP and geometrical cloud thickness decreases during the day, with a minimum around 1600 hrs, and increases at night, with a maximum at around 0700 hrs. Such variation compares well with both observations (Hignett, 1991) and previous modelling studies of the same case, e.g. Johnson *et al.* (2004).

In general, the diurnal variation exhibited by the BR-LEM simulations is the product of competition between cloud-top long-wave cooling that occurs during both day and night, and daytime solar heating. At night-time, cloud-top long-wave cooling (Figure 2(a)) creates a layer of negatively buoyant, unstable cloud-top air, which destabilises the boundary layer (Figure 2(b)), thereby causing convective overturning and the generation of turbulent kinetic energy (TKE) (Figure 2(c)). This dynamic activity results in a coupling between the cloud and the surface moisture fluxes, which causes a moist cloud layer (Figure 2(d)), thereby maintaining and enhancing night-time LWP and cloud thickness.

During the day, solar heating of the cloud diminishes the effect of cloud-top long-wave cooling (Figure 2(a)), which reduces the production of negatively buoyant air and leads to an increase in boundary-layer stability (Figure 2(b)) and a reduction in the TKE throughout the boundary layer (Figure 2(c)). As a consequence, cloud-top mixing and hence entrainment are reduced, which results in cloud-top descent (Figure 1(b)). The daytime reduction in boundary-layer dynamics causes a reduction in the moisture flux into the cloud as the cloud becomes partially decoupled from the surface and this leads to a drying of the cloud layer (Figure 2(d)). This reduction in moisture flux, along with the enhanced daytime temperatures, leads to the evaporation of the cloud and ascent of the cloud base.

Although there is this general similarity in the temporal evolution of the diurnal cycle, it is clear that increasing CCN concentrations in the BR-LEM causes a decrease in both daytime and night-time LWP (Figure 1) and a warmer and drier boundary layer (Figure 2(b, d)). Figure 3(a) demonstrates the LWP response to changes in CCN concentrations further by showing that a 100 versus 1000 cm^{-3} CCN perturbation leads to a decrease in diurnally averaged LWP of 26% on day 1 and 37% on day 2. Figure 1 also shows that the Bulk-LEM simulations produce much less variation in LWP and cloud depth, i.e. decreasing r_e from 10 to 5.5 μm leads to a LWP change of only 1% on day 1 and 8% on day 2 (Figure 3(b)). This suggests that the BR-LEM, which simulates aerosol–cloud interactions, is more responsive to changes in 'pollution' than the Bulk-LEM that has no direct representation of aerosol–cloud interactions.

Figure 4 shows that, as expected, increasing CCN concentrations in the BR-LEM results in an enhanced N_d and reduction in cloud-drop r_e. For all simulations, N_d decreases during the day and increases at night. Furthermore, the profile of N_d varies diurnally, with daytime N_d increasing with height, while at night N_d tends toward a constant vertical profile. The night-time N_d profiles for all simulations are in good agreement with the classic picture of non-precipitating stratocumulus (e.g. Noonkester, 1984). During the day, solar warming of the boundary layer completely evaporates smaller drops at the cloud base more readily than the large drops at cloud top. This results in a greater decrease in N_d at the cloud base than at cloud top and thus N_d increases with height. We note that the daytime profiles deviate from the classic N_d profile for marine Sc, i.e. constant with height (e.g. Noonkester, 1984; Wood, 2005). This is due to the fact that the simulations presented neglect sedimentation. Sedimentation would transport some of the larger drops from the top of the cloud to the base, thereby reducing the gradient in N_d. Figure 4(b, d) show that r_e increases

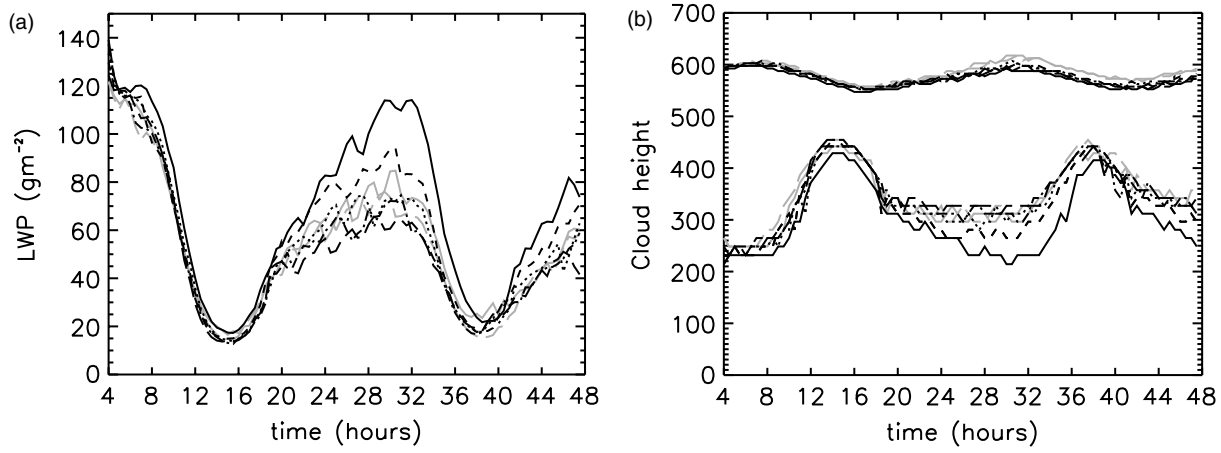

Figure 1. (a) LWP (g m^{-2}) and (b) cloud-top and cloud-base heights (m) for Bin100 (solid line), Bin250 (short dashed line), Bin500 (dotted line), Bin750 (dot-dashed line) and Bin1000 (long dashed). The grey lines show the corresponding values for Bulk10 (solid line) and Bulk5.5 (long dashed).

DOI: 10.1002/qj

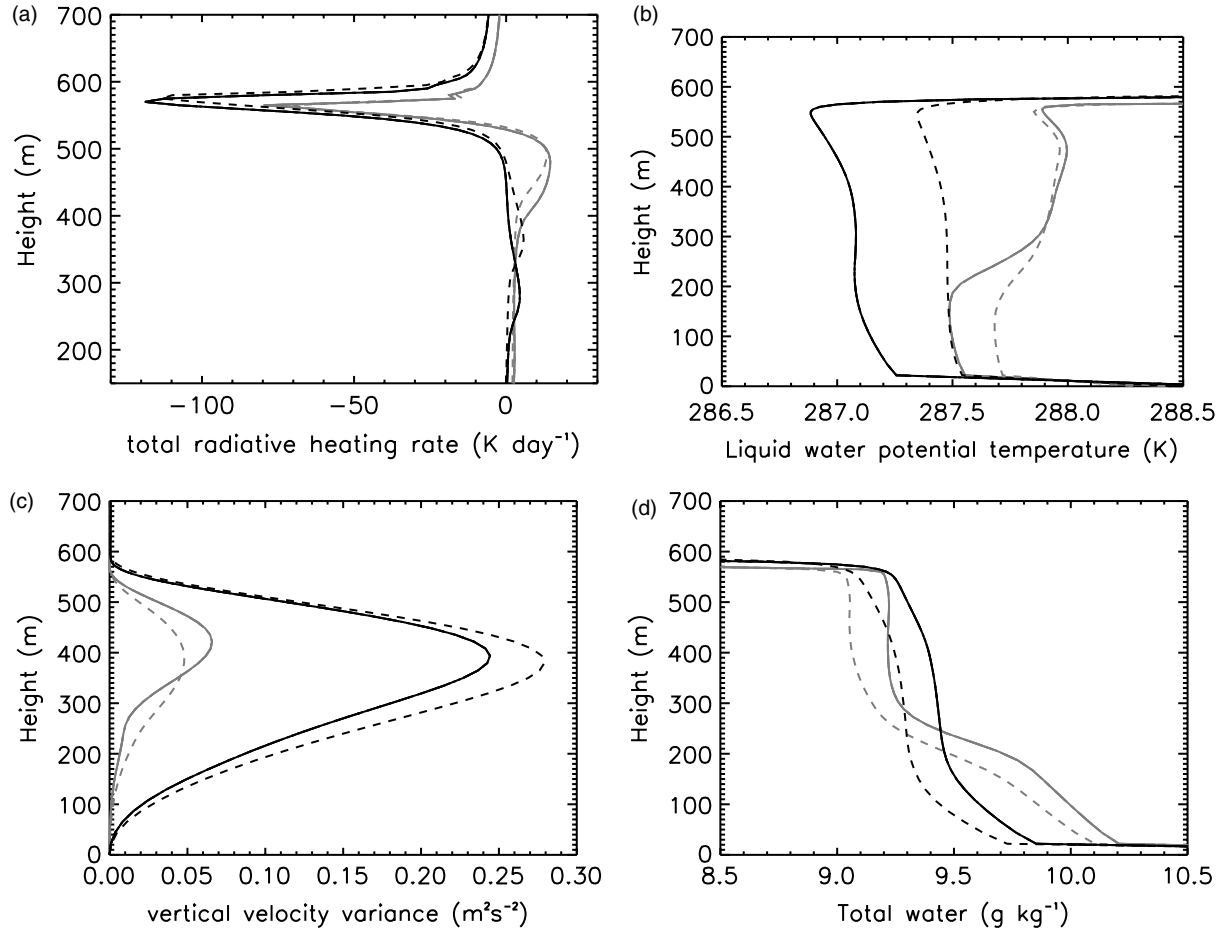

Figure 2. (a) The total radiative heating rate (K day^{-1}), (b) liquid water potential temperature (K), (c) $\overline{w'w'}$(m^{2}s^{-2}) and (d) total water (g kg^{-1}) from the Bin100 (solid line) and Bin1000 (dashed line) simulations. The grey lines represent a 3-hour average for the daytime minimum in LWP on day 2 (1400 h to 1700 h), and the black lines represent the 3-hour average for the night-time maximum in LWP on day 2 (0500 h to 0800 h).

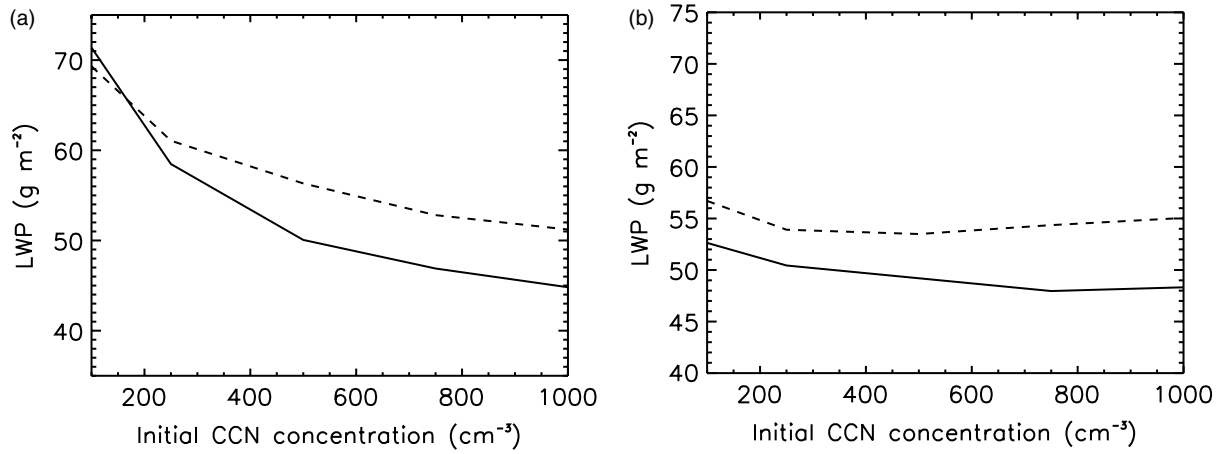

Figure 3. The diurnally averaged LWP (g m^{-2}) from (a) the BR-LEM and (b) the Bulk-LEM sensitivity studies for day 1 (dashed line) and day 2 (solid line).

with height both during the day and night and that r_e shrinks during the day and grows at night.

Thus, increasing CCN results in a reduction in r_e, as expected; however, it also produces a reduction in LWP and a warmer, drier boundary layer. A decrease in LWP with increasing CCN concentrations has been both observed (e.g. Twohy *et al.*, 2005) and noted in simulations (e.g. Wang *et al.* 2003). Within the non-precipitating framework employed here, two principle mechanisms can be envisaged that account for this CCN-induced reduction

DOI: 10.1002/qj

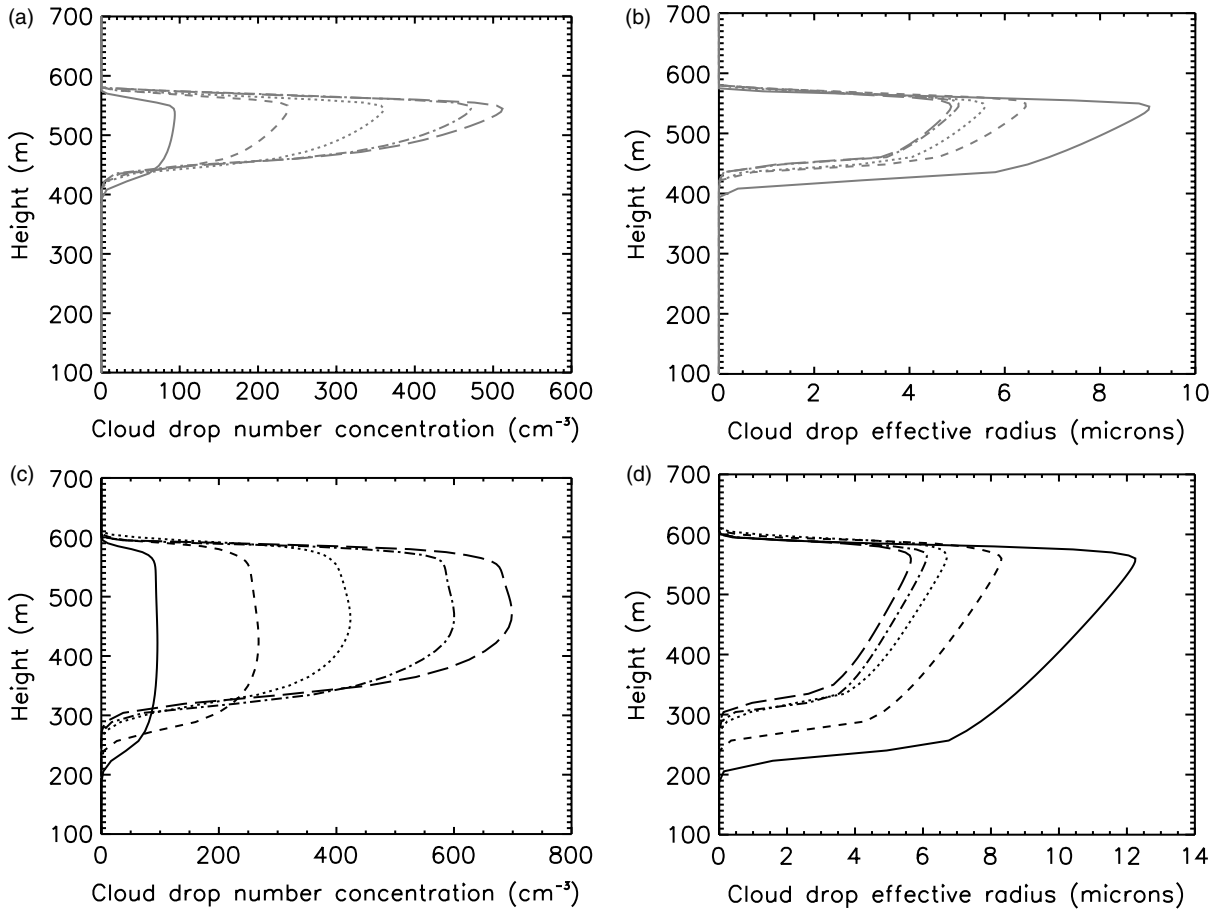

Figure 4. Horizontally averaged (a) cloud-drop number concentration and (b) cloud-drop effective radius for the daytime minimum in LWP (1400 h to 1700 h), with Bin100 (solid line), Bin250 (short dashed), Bin500 (dotted), Bin750 (dot-dashed) and Bin1000 (long dashed). (c, d) are as (a, b), but for the night-time maximum in LWP (0500 h to 0800 h day 2).

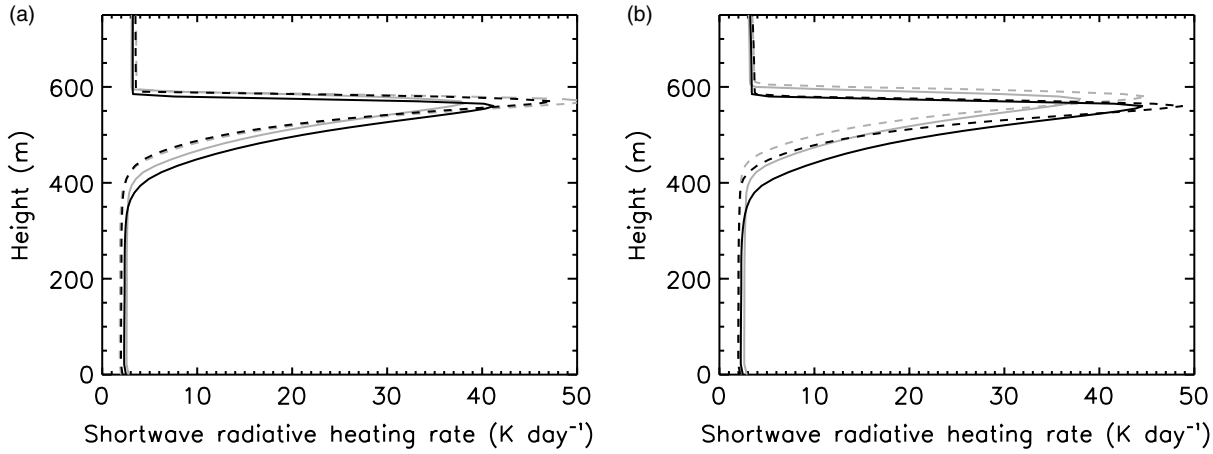

Figure 5. Short-wave heating rate (K day^{-1}) averaged over a three-hour period with maximum solar heating (1200 h to 1500 h) for (a) day 1 and (b) day 2, for simulations Bin100 (solid black lines), Bin1000 (dashed black), Bulk10 (solid grey) and Bulk5.5 (dashed grey).

in LWP and change in boundary-layer thermodynamics: (i) increasing CCN concentration results in a change in solar heating rates and/or (ii) increasing CCN concentration cause dynamical feedbacks that result in a reduction in LWP (e.g. Wang *et al.* 2003). Concerning (i), Figure 5 shows that while a reduction in r_e results in a change in the vertical distribution of solar heating, it does not account for the CCN-induced warming of the boundary layer that is demonstrated in Figure 2(b). In fact, Figure 5 shows that increasing CCN concentration results in a small decrease in sub-cloud solar warming, which is opposite to the trend shown in Figure 2(b). Figure 5 also shows that the Bulk10 and Bulk5.5 simulations produce very similar solar heating profiles, particularly in

DOI: 10.1002/qj

the sub-cloud region, to their equivalent BR-LEM simulations. This indicates that the difference between the BR-LEM and Bulk-LEM simulations (Figures 1 and 3) is not explained by differences in the short-wave heating that may result from differences in the structure of the r_e profile.

As Figure 5 indicates that changes in short-wave heating that result from increases in CCN do not explain the simulated change in LWP and boundary-layer thermodynamics, our attention turns to the role of dynamical feedbacks. Wang *et al.* (2003) used numerical simulation of nocturnal non-precipitating marine Sc to demonstrate that the smaller drops that result from higher CCN concentrations evaporate more readily, causing increased cloud-top entrainment rates and a reduction in LWP, i.e. a similar response to that demonstrated in the BR-LEM diurnal simulations. This process has since been termed the 'evaporation–entrainment' feedback (Xue and Feingold, 2006) and it has been shown to counteract the increases in LWP and cloud fraction associated with suppression of precipitation in cumulus clouds (Xue and Feingold, 2006; Jiang *et al.*, 2006). Figure 6(a) demonstrates that, as suggested by Wang *et al.* (2003), increasing CCN concentration results in an increase in the cloud-top evaporation rate. This drives stronger boundary-layer dynamics (Figure 6(b)), which in turn cause a higher entrainment rate. For example, during the morning when the simulations are minimally affected by solar radiation (the period shown in Figure 6), Bin100 produces an entrainment rate of 0.33 cms^{-1}, while Bin1000 produces an entrainment rate of 0.39 cms^{-1}. This enhanced entrainment rate causes more mixing of warm, dry air from above the boundary layer, thereby warming and drying the boundary layer, relative to the clean simulation (Figure 2(b, d), respectively), which in turn leads to a reduction in LWP.

Figure 6 also presents an example of one of the Bulk-LEM simulation (Bulk10). Irrespective of r_e, the Bulk-LEM simulations employ an 'all-or-nothing' condensation–evaporation (CE) scheme with an instantaneous CE rate (Section 2.1). This means that the Bulk-LEM simulations produce the maximum cloud-top evaporation rate (Figure 6(a)), which in turn leads to the strongest boundary-layer dynamics compared with the BR-LEM simulations (Figure 6(b)). It is noted that, as shown in previous work (e.g. Kogan and Martin, 1994; Wang *et al.* 2003), the CE rate of the Bulk-LEM is representative of the most polluted cloud. This is the case irrespective of the specified r_e. Hence although the specified r_e may represent differing levels of pollution in the radiative transfer calculations, the CE rate and LWP will always represent a polluted marine Sc.

While Figure 6 demonstrates the occurrence of the evaporation–entrainment feedback during the early morning of the BR-LEM simulations, the boundary-layer warming and drying associated with the greater entrainment is seen throughout the simulation (Figure 2(b, d)), with the largest response in LWP at night-time. This large night-time response is the result of a change in the sub-cloud stability, with the enhanced entrainment warming associated with an increase in sub-cloud stability. For example, during early evening when the LWP is recovering from daytime dessication, the sub-cloud $d\theta/dz$ in simulation Bin100 is -9.2×10^{-3} K m^{-1}, while $d\theta/dz$ in Bin1000 is -2.2×10^{-3} K m^{-1}. This enhancement of sub-cloud stability with increases in CCN concentration results in a reduction of the vapour flux into the cloud (Figure 7), which in turn causes a lower night-time LWP. During the daytime, particularly around the daytime minimum, the influence of the evaporation–entrainment feedback on LWP becomes less obvious because the boundary-layer dynamics, and hence LWP, are dominated by the stabilising effect of the solar warming.

The response of LWP to changes in CCN concentrations is important because cloud optical depth, τ, is dependent on both LWP and N_d. Figure 8 shows the day 2 diurnally averaged τ and the τ averaged over the sunlight hours (0700 to 2000) from the BR-LEM. Irrespective of the averaging period, increasing CCN

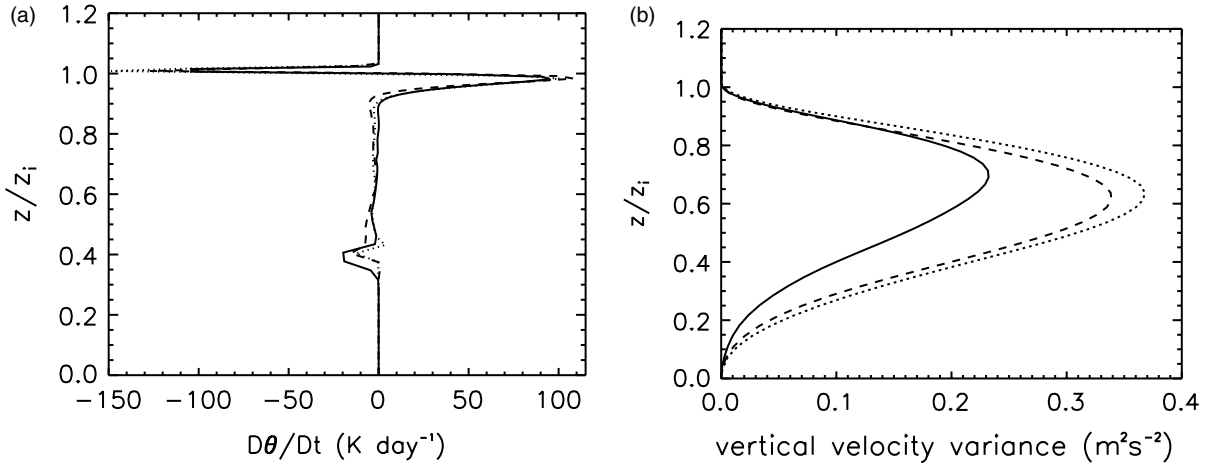

Figure 6. (a) The mean condensation–evaporation rate (K day^{-1}) and (b) the mean $\overline{w'w'}$ (m^2 s^{-2}) for Bin100 (solid line), Bin1000 (dashed) and Bulk10 (dotted). Both plots show a two-hour average for 0600 h to 0800 h, during which LWP are approximately equal and the boundary layer has not been strongly influenced by solar warming.

DOI: 10.1002/qj

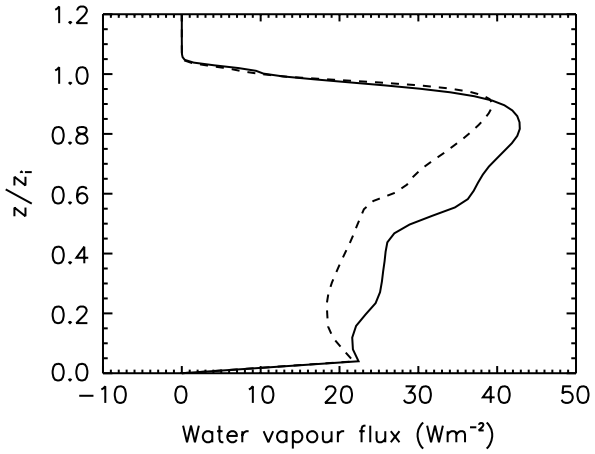

Figure 7. The average latent heat flux (W m^{-2}) from Bin100 (solid line) and Bin1000 (dashed) for the cloud recovery period, 2000 h to 2300 h, during which LWP and cloud depth increase.

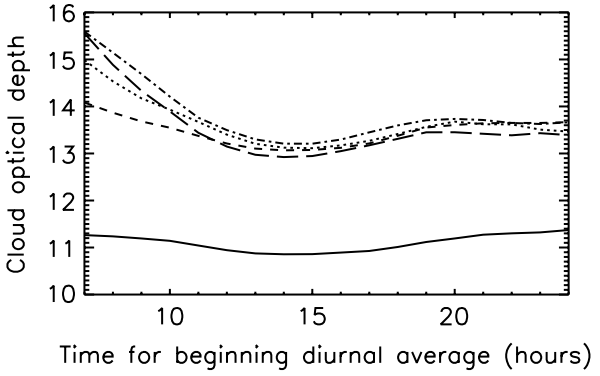

Figure 9. Diurnally averaged cloud optical depth, τ, calculated every hour from 0700 h to 2400 h on day 1. The line descriptions are as Figure 1.

concentrations in the BR-LEM leads to an increase in τ (Figure 8(a)), which is an expected response. However, while increasing CCN concentrations from 100 to 250 cm^{-3} produces a 17% increase in τ, increasing CCN above 250 cm^{-3} results in no significant change in τ, i.e. no more than 1%. The lack of sensitivity of τ exhibited by the more polluted clouds is the result of the decrease in LWP with increasing CCN concentrations (Figure 3(a)), which reduces the change in τ that would be expected for the reduction in r_e. In contrast, specifying a smaller r_e in the Bulk-LEM simulations results in very little variation in LWP (Figure 3(b)). As a result, τ tends to increase with a reduction in r_e (Figure 8(b)).

Figure 8 presents only day 2 averages as these are less influenced by initial conditions. This is shown in Figure 9 where it is clear that calculating the diurnally averaged τ, i.e. a 24-hour average, with a start time for the averaging period between 0700 and 1200 hours on day 1, results in much larger diurnally averaged τ than if the average were calculated after 1200 hours on day 1. Thus, although LWP decreases from day 1 to day 2, Figure 9 indicates that the diurnally averaged τ approaches equilibrium when calculated after 1200 hours. From Figure 9, it is reasonable to expect that a day 3 diurnally averaged τ for each CCN distribution would be similar to the day 2 average presented in Figure 8.

Therefore, the BR-LEM simulations clearly demonstrate the evaporation–entrainment feedback and Figure 8 shows that this can have a significant influence on the response of τ to increases in CCN. While Wang *et al.* (2003) demonstrated the evaporation–entrainment feedback in nocturnal marine Sc, the results presented here show that it has a strong influence on diurnally varying marine Sc, which in turn can play an important role in determining the response of the cloud optical properties.

3.3. The indirect radiative forcing

In this section we present estimates of the local indirect forcing for the simulations presented. These estimates have been computed using the definition suggested by McFarquhar and Wang (2006). The indirect forcing, f_{indirect}, is defined as follows

$$f_{\text{indirect}} = F_{\text{net}}(\text{polluted cloud}) - F_{\text{net}}(\text{clean cloud}), \quad (1)$$

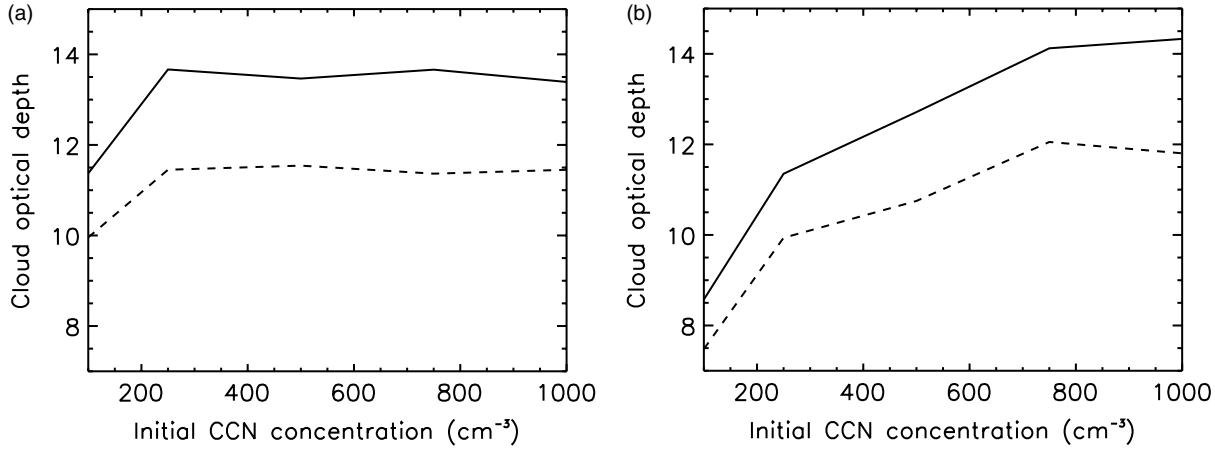

Figure 8. The diurnally averaged cloud optical depth, τ (solid line), and the daylight-hour average (0700 h to 2000 h; dashed) from the (a) BR-LEM and (b) Bulk-LEM sensitivity studies for day 2.

DOI: 10.1002/qj

where F_{net} is the net flux (downwelling flux minus upwelling flux) for the separate simulations in which the clean cloud is Bin100 in BR-LEM simulations (or Bulk10 in the Bulk-LEM simulations). The polluted simulations refer to increasing CCN in the BR-LEM (or reducing cloud-drop r_e in the Bulk-LEM).

Figure 10 shows that all simulations produce top-of-the-atmosphere (TOA) indirect forcing estimates that are negative, with increasing CCN concentrations (or specifying a smaller r_e) causing an increase in the magnitude of the indirect forcing. However, Figure 10 shows that increasing CCN concentrations in the BR-LEM produces a forcing that is 60% weaker in magnitude (on day 2) than that produced by decreasing r_e in the Bulk-LEM.

The previous section has demonstrated two major differences between the BR-LEM and Bulk-LEM simulations, which can impact the change in τ and hence the indirect forcing. First, increasing CCN concentration in the BR-LEM produces an evaporation–entrainment feedback that results in a reduction in the LWP. This process is not captured in the Bulk-LEM. Second, all the BR-LEM experiments demonstrate that both r_e and N_d vary diurnally, yet in the Bulk-LEM cloud-drop r_e is assumed to be constant during the simulation. Using offline radiative calculations, it is possible to understand the radiative impact of LWP and r_e changes independent from the cloud responses. The input for these calculations were the 1D horizontally and time-averaged vertical profiles, which were output every 30 minutes during the BR-LEM. These profiles were used to simulate the diurnal cycle in radiative fluxes that is associated with diurnal variation in marine Sc obtained from either model.

Using the BR-LEM profiles, we established three sets of simulations (Table III). Set 1, the control, contains the offline simulations that employ the most restrictive assumptions in which r_e does not vary during the day, the assumption of the Bulk-LEM, and LWC does not vary with increased pollution. This set of simulations employ vertical profiles obtained from the Bin100 simulation, while the r_e is set to be equal to the r_e used in the Bulk-LEM experiments. Set 2 employs the assumption that LWP does not vary with increased pollution, but relaxes the fixed r_e assumption by employing the diurnally varying cloud-top r_e from the BR-LEM simulation. Comparison of Set 1 and Set 2 is used to quantify the change in radiative forcing associated with permitting r_e to vary. Set 3 relaxes both the assumptions of Sets 1 and 2 by employing the LWC from each BR-LEM experiment with the associated diurnally varying cloud-top r_e. Comparison of Set 3 and Set 2 is used to quantify the change in radiative forcing associated with permitting variability in LWP with increasing CCN concentrations.

Table III. Outline of the offline radiative transfer simulations that have been performed to understand the differences in the indirect forcing produced by the BR-LEM and the Bulk-LEM.

Experiment	CCN conc. (cm^{-3})	Description	
		LWC	r_e
Set 1	100	Bin100	10.0 μm
Control	250	Bin100	7.4 μm
	500	Bin100	6.4 μm
	750	Bin100	5.65 μm
	1000	Bin100	5.5 μm
Set 2	100	Bin100	Bin100
LWC fixed,	250	Bin100	Bin250
with diurnally	500	Bin100	Bin500
varying			
cloud-top r_e	750	Bin100	Bin750
	1000	Bin100	Bin1000
Set 3	100	Bin100	Bin100
LWC variable,	250	Bin250	Bin250
with diurnally	500	Bin500	Bin500
varying			
cloud-top r_e	750	Bin750	Bin750
	1000	Bin1000	Bin1000

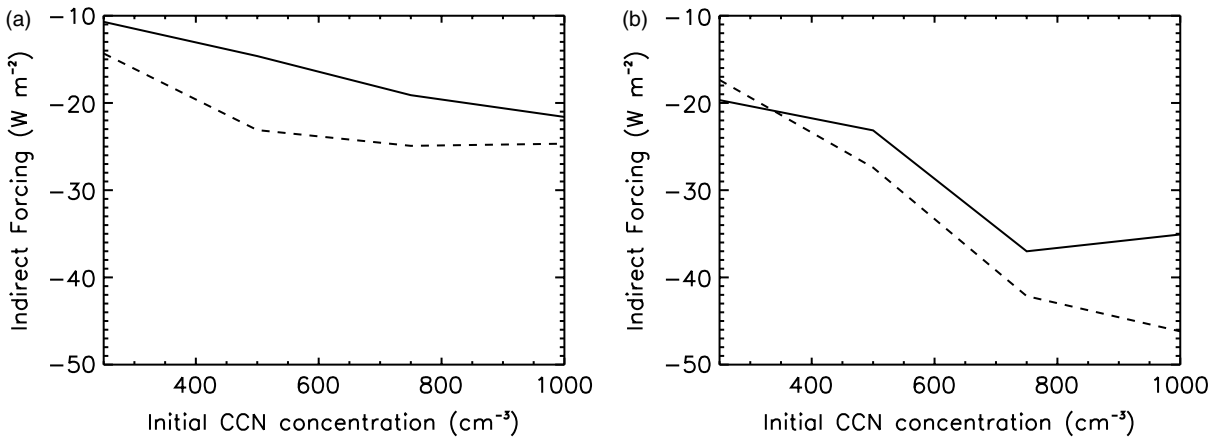

Figure 10. The diurnally averaged indirect TOA forcing (W m^{-2}) from (a) the BR-LEM and (b) the Bulk-LEM. The day 1 average is the dashed line, and the day 2 average is the solid line.

DOI: 10.1002/qj

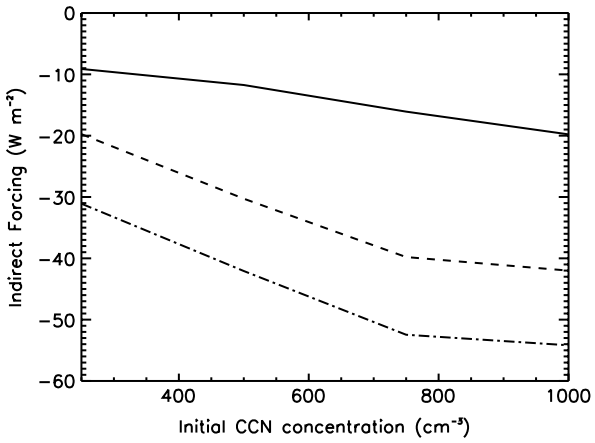

Figure 11. The TOA indirect forcing (W m^{-2}) produced by the sensitivity tests detailed in Table III. The dot-dashed line shows Set 1 (control with LWC fixed and r_e specified), the dashed line shows Set 2 (fixed LWC and diurnally varying r_e) and the solid line shows Set 3 (LWC varying with increased CCN and r_e varying diurnally).

Figure 11 shows the forcing resulting from the offline radiative transfer calculations. Comparison of Set 1 simulations with Set 2 and 3 simulations demonstrates that assuming a constant r_e and LWP with increasing CCN leads to the largest magnitude in indirect forcing estimates. In fact, it is clear that employing the assumptions of Set 1 result in a indirect forcing in marine Sc that is triple that generated when r_e and LWP are permitted to vary (Set 3). Comparison of Set 2 simulations with Set 1 shows that permitting the r_e to vary diurnally results in a reduction in the magnitude of the indirect forcing of approximately 10 W m^{-2}. This reduction in forcing is approximately the same for all CCN concentrations, which suggests that the reduction in the forcing associated with a varying r_e is independent of the initial CCN concentration.

Comparison of Set 3 simulations with Set 2 shows that allowing LWP to respond to increased CCN produces a further reduction in the magnitude of the indirect forcing. However, unlike permitting only r_e to vary (Set 2), this reduction is dependent on the CCN concentration. For example, the change in LWP that results from increasing CCN concentration to 250 cm^{-3} causes a 10.5 W m^{-2} reduction in indirect forcing, relative to Set 2. This reduction in forcing is approximately equal to the reduction in indirect forcing that results from permitting r_e to vary. In contrast, increasing CCN concentration to 1000 cm^{-3} produces a 23 W m^{-2} reduction in indirect forcing, relative to Set 2. This is over double the reduction in indirect forcing that results from permitting r_e to vary.

Therefore, both the diurnal variation in r_e and variation in LWP with increased CCN act to reduce the magnitude of the indirect forcing estimate and both processes are required to prevent an overestimation of the indirect forcing. However, as the marine Sc becomes more polluted, reduction in the LWP with increased CCN concentrations becomes twice as important in determining the indirect forcing. It has been shown that the change in LWP with increasing CCN concentrations in the BR-LEM is the product of an evaporation–entrainment feedback. Figure 11 suggests that the omission of such a process in the very polluted simulations would result in a doubling of the indirect forcing estimate for the most polluted case.

4. Summary and conclusion

In this paper we describe the integration of a detailed size-bin-resolved cloud microphysical scheme into the UKMO LEM to create the BR-LEM. We have used the BR-LEM to investigate how changes in CCN concentration influence diurnally varying non-precipitating marine Sc and hence the indirect forcing. As a comparison, we also performed simulations with the microphysically simpler standard Bulk-LEM.

It is found that while increasing CCN concentrations in the BR-LEM results in a reduction in r_e, it also results in up to a 37% reduction in diurnally averaged LWP. This reduction in LWP results from an evaporation–entrainment feedback, which drives stronger boundary-layer dynamics, leading to more entrainment drying of the boundary layer and lower LWP. This agrees with Wang *et al.* (2003), who demonstrated such a feedback in 6-hour simulations of nocturnal marine Sc. At the end of their paper, Wang *et al.* (2003) asked 'How much does the feedback contribute to the overall impact of the changing CCN number concentration?'. In this paper we have shown that, although the LWP response to the evaporation–entrainment feedback is most obvious at night, the associated warming and drying of the boundary layer is clear throughout the day and night, which results in a reduction in daytime LWP. This in turn significantly reduces the response of τ to changes in CCN concentrations, i.e. increasing CCN from 250 to 1000 cm^{-3} results in no more than 1% change in τ, in the case presented. By using offline radiation calculations, we have shown that ignoring the change in LWP with increasing CCN concentration can result in a doubling of the indirect forcing estimate. Thus, for the case presented, the evaporation–entrainment feedback associated with increasing CCN concentrations can play a significant role in the estimation of the indirect forcing in marine Sc.

In contrast to the BR-LEM, approximating a change in CCN concentration in the Bulk-LEM, by reducing the specified r_e produces much less variation in the LWP, i.e. less than 10% change in LWP. The Bulk-LEM employs an 'all-or-nothing' condensation–evaporation scheme, with an instantaneous CE rate. Such a simple scheme fails to produce the CCN-induced changes in CE rate and hence fails to produce the dynamic responses and the LWP changes associated with increases in CCN. While such a difficiency within an 'all-or-nothing' bulk microphysics scheme has been shown in previous work (e.g. Kogan and Martin, 1994; Wang *et al.* 2003), this work highlights that the assumption of an instantaneous CE rate can result in a significant error in the simulated

DOI: 10.1002/qj

LWP in diurnally varying marine Sc, and the indirect effect.

Ackerman *et al.* (2004) demonstrated that increasing CCN concentrations in microphysically more complicated precipitating clouds also results in an entrainment feedback that can, depending on conditions, reduce LWP and hence obscure the indirect effect. While this work neglects precipitation processes, it demonstrates that dynamical feedbacks associated with non-precipitating processes can influence marine Sc and also obscure the indirect effect. This further highlights the importance of capturing the coupling between changes in CCN concentrations, microphysics and dynamics when investigating the indirect aerosol effect.

Acknowledgements

We would like to thank the Natural Environment Research Council (NERC) for funding AH and the UK Met Office for providing the large-eddy model (LEM). We would like to thank Jason Lander and James Groves for their assistance with setting up the LEM, and Martyn Chipperfield and John Marsham for their helpful comments during this work.

References

Ackerman AS, Toon OB, Stevens DE, Heymsfield AJ, Ramanathan V, Welton EJ. 2000. Reduction of tropical cloudiness by soot. *Science* **288**: 1042–1047.

Ackerman AS, Kirkpatrick MP, Stevens DE, Toon OB. 2004. The impact of humidity above stratiform clouds on indirect aerosol climate forcing. *Nature* **432**: 1014–1017.

Albrecht B. 1989. Aerosols, cloud microphysics, and fractional cloudiness. *Science* **245**: 1227–1230.

Dobbie S, Jonas P. 2001. Radiative influences on the structure and lifetime of cirrus clouds. *Q. J. R. Meteorol. Soc.* **127**: 2663–2682.

Feingold G, Tzivion S, Levin Z. 1988. Evolution of raindrop spectra. Part I: Stochastic collection/breakup using the method of moments. *J. Atmos. Sci.* **45**: 3387–3399.

Feingold G, Jiang H, Harrington JY. 2005. On smoke suppresion of clouds in Amazonia. *Geophys. Res. Lett.* **32**: L02804, DOI:10.1029/2004GL021369.

Fu Q, Liou KN. 1993. Parameterization of the radiative properties of cirrus clouds. *J. Atmos. Sci.* **50**: 2008–2025.

Gray MEB, Petch J, Derbyshire SH, Brown AR, Lock AP, Swann HA, Brown PRA. 2001. 'Version 2.3 of the Met Office large-eddy model: Part II. Scientific documentation'. APR Turbulence and Diffusion note 276. Met Office: Exeter, UK.

Hansen JE, Sato M, Ruedy R. 1997. Radiative forcing and climate response. *J. Geophys. Res.* **102**: 6831–6864.

Hignett P. 1991. Observations of diurnal variation in a cloud-capped marine boundary layer. *J. Atmos. Sci.* **48**: 1474–1482.

IPCC 2007. *Climate Change 2007: The scientific basis. Third assessment report of the Intergovernmental Panel on Climate Change.* Cambridge University Press: Cambridge, UK and New York.

Ivanova ET, Kogan YL, Mazin IP, Permyakov MS. 1977. Method of parameterizing the condensation process of droplet growth in numerical cloud models. *Izv. Akad. Sci. USSR. Atmos. Ocean. Phys.* **14**: 617–623.

Jiang H, Xue H, Teller A, Feingold G, Levin Z. 2006. Aerosol effects on the lifetime of shallow cumulus. *Geophys. Res. Lett.* **33**: DOI:10.1029/2006GL026024.

Johnson BT, Forster PM, Shine KP. 2004. The semi-direct aerosol effect: Impact of absorbing aerosol on marine stratocumulus. *Q. J. R. Meteorol. Soc.* **130**: 1407–1422.

Khain A, Ovtchinnikov M, Pinksky M, Pokrovsky A, Krugliak H. 2000. Notes on the state-of-the-art numerical modeling cloud microphysics. *Atmos. Res.* **55**: 159–224.

Kogan YL. 1991. The simulation of a convective cloud in a 3-D model with explicit microphysics. Part I: Model descriptions and sensitivity experiments. *J. Atmos. Sci.* **48**: 1160–1189.

Kogan YL, Martin WJ. 1994. Parameterization of bulk condensation in mumerical cloud models. *J. Atmos. Sci.* **51**: 1727–1739.

Kogan YL, Khairoutdinov MP, Lilly DK, Kogan ZN, Liu Q. 1995. Modeling of stratocumulus cloud layers in a large-eddy simulation model with explicit microphysics. *J. Atmos. Sci.* **52**: 2923–2940.

Lu M-L, Seinfeld JH. 2005. Study of the aerosol indirect effect by large-eddy simulation of marine stratocumulus. *J. Atmos. Sci.* **62**: 3909–3932.

McFarquhar GM, Wang H. 2006. Effects of aerosols on trade-wind cumuli over the Indian Ocean: Model simulations. *Q. J. R. Meteorol. Soc.* **132**: 821–843.

Noonkester VR. 1984. Droplet spectra observed in marine stratus cloud layers. *J. Atmos. Sci.* **41**: 829–845.

Raes F, Van Dingenen R, Vignati E, Wilson J, Putaud J-P, Seinfeld JH, Adams P. 2000. Formation and cycling of aerosols in the global troposphere. *Atmos. Environ.* **34**: 4215–4240.

Ramanathan V, Crutzen PJ, Kiehl JT, Rosenfeld D. 2001. Aerosols, climate and the hydrological cycle. *Science* **294**: 2119–2124.

Twohy CH, Petters MD, Snider, Jefferson SR, Stevens B, Tahnk W, Wetzel M, Russell L, Burnet F. 2005. Evaluation of the aerosol indirect effect in marine stratocumulus clouds: Droplet number, size, liquid water path, and radiative impact. *J. Geophys. Res.* **110**: DOI:10.1029/2004JD005116.

Twomey S. 1991. Aerosols, clouds, and radiation. *Atmos. Environ.* **25**: 2435–2442.

Tzivion S, Feingold G, Levin Z. 1987. An efficient numeric solution to the stochastic collection equation. *J. Atmos. Sci.* **44**: 3139–3149.

Tzivion S, Feingold G, Levin Z. 1989. The evolution of raindrop spectra. Part II: Collisional collection/breakup and evaporation in a rainshaft. *J. Atmos. Sci* **46**: 3312–3127.

Wang S, Wang Q, Feingold G. 2003. Turbulence, condensation, and liquid water transport in numerically simulated nonprecipitating stratocumulus clouds. *J. Atmos. Sci.* **60**: 262–278.

Wood R. 2005. Drizzle in stratiform boundary layer clouds. Part I: Vertical and horizontal structure. *J. Atmos. Sci.* **62**: 3011–3033.

Xue H, Feingold G. 2006. Large-eddy simulations of trade wind cumuli: Investigation of aerosol indirect effects. *J. Atmos. Sci.* **63**: 1605–1622.

Yin Y, Levin Z, Reisin TG, Tzivion S. 2000. The effects of giant cloud condensation nuclei on the development of precipitation in convective clouds – A numerical study. *Atmos. Res.* **53**: 91–116.

Yin Y, Carslaw KS, Feingold G. 2005. Vertical transport and processing of aerosol in a mixed-phase convective cloud and the feedback on cloud development. *Q. J. R. Meteorol. Soc.* **131**: 221–245.